Letter

Chirality inversion and radius blowup of a Néel-type skyrmion by a Pearl vortex

S. S. Apostoloff,[1,2] E. S. Andriyakhina,[3,1] P. A. Vorobyev,[4] Oleg A. Tretiakov,[4] and I. S. Burmistrov[1,2,*]

[1]*L. D. Landau Institute for Theoretical Physics, Semenova 1-a, 142432, Chernogolovka, Russia*

[2]*Laboratory for Condensed Matter Physics, HSE University, 101000 Moscow, Russia*

[3]*Moscow Institute for Physics and Technology, 141700 Moscow, Russia*

[4]*School of Physics, The University of New South Wales, Sydney 2052, Australia*

(Received 16 December 2022; accepted 14 June 2023; published 30 June 2023)

We develop a theory for the coaxial configuration of a Néel-type skyrmion and a Pearl vortex in thin superconductor-chiral ferromagnetic heterostructures. Using an exact numerical solution of the Euler-Lagrange equation and micromagnetic simulations, we demonstrate that the inhomogeneous magnetic field of the Pearl vortex significantly modifies the skyrmion profile with respect to the same profile in the absence of the vortex. We discover drastic enlargement of the radius of the skyrmion and inversion of the chirality of the skyrmion. To unravel the physics behind these effects, we invent a two-parameter ansatz for the magnetization profile of the skyrmion in the presence of the vortex. Chirality inversion and radius blowup are controlled not only by the material parameters of the heterostructure but also by the thickness of the superconductor. Our findings can have implications for Majorana modes localized at skyrmion-vortex pairs.

DOI: 10.1103/PhysRevB.107.L220409

I. INTRODUCTION

Interest in the coexistence of magnetism and superconductivity in heterostructures has resurged over the last two decades [1–5]. Superconductor–chiral ferromagnet (SF) bilayers have recently attracted a great deal of attention [6–8] due to their potential to exhibit two topologically nontrivial configurations: (i) skyrmions stabilized by the Dzyaloshinskii-Moriya interaction (DMI) in a ferromagnetic film [9], and (ii) vortices in a superconductor. Skyrmions in SF bilayers demonstrate rich physics, as they can induce Yu-Shiba-Rusinov-type bound states [10,11], modify the Josephson effect [12], and change the superconducting critical temperature [13]. Skyrmion-vortex pairs host Majorana modes [14–21] and can serve as a scalable topological quantum computing platform [22]. An experimental demonstration of stable skyrmion-vortex coexistence has been recently reported in a $[Ir_1Fe_{0.5}Co_{0.5}Pt_1]^{10}$/MgO/Nb sandwich [23].

Skyrmions and vortices in SF bilayers can form bound pairs due to the interplay of spin-orbit coupling and thr proximity effect [24,25] as well as due to their interaction via the magnetic stray fields [26–29]. Traditionally, analysis of Majorana modes in skyrmion-vortex pairs ignores the effect of stray fields. However, for a thin SF bilayer, the interaction due to stray fields results in a dramatic effect: Repulsion of a Néel-type skyrmion from a Pearl vortex to a finite distance stable position [29].

In this letter, we develop a theory for the coaxial configuration of a Néel-type skyrmion and a Pearl vortex in a thin SF heterostructure. We use two complementary approaches: Exact numerical solution of the Euler-Lagrange equation, cf. Eq. (3), and micromagnetic simulations based on the Landau-Lifshitz-Gilbert equation. To perform the free energy minimization, we invent a two-parameter ansatz, cf. Eq. (5), inspired by exact numerical solutions of the Euler-Lagrange equation. We create this anzatz based on naturally arising synergy of the profile of a sole skyrmion and the magnetization induced by the vortex. We find that the inhomogeneous magnetic field of the Pearl vortex significantly modifies the profile of the skyrmion and results in two effects: (i) drastic enlargement of the radius of the skyrmion with respect to that in the absence of the vortex and (ii) inversion of the chirality with respect to the natural chirality fixed by the sign of the DMI. Both effects can have implications for the existence of Majorana modes localized at skyrmion-vortex pairs.

II. MODEL

We consider a heterostructure consisting of two films, superconducting and ferromagnetic, separated by a thin insulating layer (of thickness $\ll\lambda_L$) that suppresses the proximity effect. The superconducting film is assumed to be much thinner than the London penetration depth, $d_S\ll\lambda_L$, and to contain a Pearl vortex. The main goal of this letter is to study the situation in which a Néel-type skyrmion in the ferromagnetic film is located directly above (i.e., coaxially) a Pearl vortex in the superconducting film.

The free energy of a thin chiral ferromagnetic film interacting with a Pearl vortex is given by

$$\mathcal{F}[\mathbf{m}] = d_F \int d^2\mathbf{r}\big\{A(\nabla\mathbf{m})^2 + K\big(1-m_z^2\big) + D[m_z\nabla\cdot\mathbf{m} - (\mathbf{m}\cdot\nabla)m_z] - M_s\mathbf{m}\cdot\mathbf{B}_V|_{z=+0}\big\}. \tag{1}$$

*burmi@itp.ac.ru

Here, $\mathbf{m}(\mathbf{r})$ is the unit magnetization vector, M_s is the saturation magnetization, and d_F is the thickness of the ferromagnetic film. Parameters $A > 0$, $K > 0$, and D stand for the exchange, effective perpendicular anisotropy [30], and DMI constants, respectively. The z axis is directed perpendicularly to the film. The magnetic field due to the Pearl vortex $\mathbf{B}_\mathrm{V}$ is centered at the origin:

$$\mathbf{B}_\mathrm{V} = \phi_0 \mathrm{sgn}(z) \nabla \int \frac{d^2\mathbf{q}}{(2\pi)^2} \frac{e^{-q|z|+i\mathbf{qr}}}{q(1+2q\lambda)}, \tag{2}$$

where $\phi_0 = hc/2e$ is the flux quantum and $\lambda = \lambda_L^2/d_S$ is the Pearl length (see Refs. [31,32] and the Supplemental Material [33]). The free energy $\mathcal{F}[\mathbf{m}]$ is normalized in such a way that $\mathcal{F} = 0$ for the ferromagnetic state ($m_z = 1$) in the absence of the Pearl vortex ($\mathbf{B}_\mathrm{V} = 0$).

Due to the radial symmetry of the problem, the magnetization of the Néel-type skyrmion coaxial with the Pearl vortex can be written as $\mathbf{m} = \mathbf{e}_r \sin\theta(r) + \mathbf{e}_z \cos\theta(r)$. Minimizing the free energy $\mathcal{F}[\mathbf{m}]$ with respect to the skyrmion angle $\theta(r)$, one can derive the Euler-Lagrange equation:

$$\frac{\ell_w^2}{r}\partial_r[r\partial_r\theta(r)] - \frac{(\ell_w^2 + r^2)}{2r^2}\sin 2\theta(r) + 2\epsilon\frac{\sin^2\theta(r)}{r/\ell_w} + \gamma[b_z(r)\sin\theta(r) - b_r(r)\cos\theta(r)] = 0, \tag{3}$$

where $\ell_w = \sqrt{A/K}$ is the domain wall width. In Eq. (3), we have two dimensionless parameters: The DMI strength $\epsilon = D/2\sqrt{AK}$ and the effective strength of the Pearl vortex $\gamma = (\ell_w/\lambda)(M_s\phi_0/8\pi A)$. The functions $b_r(r)$ and $b_z(r)$ are the rescaled projections of the magnetic field of the Pearl vortex in the ferromagnetic film $\mathbf{B}_V|_{z=+0} = -(\phi_0/4\pi\ell_w\lambda)[b_r(r)\mathbf{e}_r + b_z(r)\boldsymbol{e}_z]$.

Equation (3) should be accompanied by appropriate boundary conditions. The first boundary condition $\theta(r \to \infty) = 0$ accounts for the fact that, far from the origin, where the vortex and the skyrmion are situated, the magnetization is uniform, i.e., $m_z = 1$. The second boundary condition describes the magnetization at $r = 0$ and depends on the particular system configuration. The possible configurations are described in detail below.

A. Vortex without skyrmion

If the condition $\theta(r = 0) = 0$ is assumed, the solution $\theta(r) = \theta_\gamma(r)$ of Eq. (3) describes the magnetization of an initially homogeneous ferromagnetic film in the absence of any skyrmion in the magnetic field of the Pearl vortex. In this letter, we focus on the most realistic case in which the Pearl length λ is much larger than the skyrmion radius. In that case, both the rescaled magnetic field of the vortex and the magnetization angle $\theta(r)$ need only be considered at distances $r \ll \lambda$. In that approximation, $b_r(r) \approx b_z(r) \approx \ell_w/r$ [34], and the solution of Eq. (3) with the boundary condition $\theta(r = 0) = 0$ can be expressed analytically as [35]

$$\theta_\gamma(r) \approx \gamma\left[K_1\left(\frac{r}{\ell_w}\right) - \frac{\ell_w}{r}\right], \quad \gamma \lesssim 1, \tag{4}$$

where $K_1(x)$ is the modified Bessel function of the second kind.

B. Skyrmion with vortex

If we impose the condition $\theta(r = 0) = \chi\pi$ with $\chi = \pm 1$, the solution of Eq. (3) corresponds to a skyrmion with chirality χ. The chirality $\chi = +1$ (-1) means that the in-plane projection of the magnetization is directed from (to) the center of the skyrmion. As is well known [36], without the Pearl vortex $\gamma = 0$, the only solution of Eq. (3) exists for $|\epsilon| < 2/\pi$ [37] and has a single chirality $\chi = \mathrm{sgn}(\epsilon)$. It should be emphasized that, in the presence of the vortex $\gamma > 0$, solutions of Eq. (3) with single or both chiralities $\chi = \pm 1$ can be found depending on the magnitudes of γ and ϵ.

The exact solution of Eq. (3) with the boundary condition $\theta(r{=}0) = \chi\pi$ can be found numerically, e.g., by the shooting method. This procedure is computationally expensive because the shooting parameter must be determined to exponentially high accuracy compared with the solution itself. However, an approximate solution can be found using an alternative method, which is convenient both for numerical computations and analytical study.

C. Skyrmion-vortex ansatz

To describe the skyrmion-vortex coaxial pair, we propose using the following ansatz:

$$\theta_{R,\delta,\gamma}(r) = \theta_{R,\delta}(r) + \theta_\gamma(r)\cos\theta_{R,\delta}(r), \tag{5}$$

which is a modified version of the well-known 360° domain wall ansatz:

$$\theta_{R,\delta}(r) = 2\arctan\frac{\sinh(R/\delta)}{\sinh(r/\delta)}. \tag{6}$$

By replacing $\theta(r)$ with this modified skyrmion angle $\theta_{R,\delta,\gamma}(r)$ in the free energy, $\mathcal{F}[\mathbf{m}]$ can then be minimized with respect to two parameters only: R and δ. While the latter plays the role of the skyrmion wall width, the former encodes both the skyrmion chirality $\chi = \mathrm{sgn}R$ and its radius $|R|$.

The qualitative idea of the construction of the ansatz in Eq. (5) is as follows. One may expect that the skyrmion magnetization shape is described by the 360° domain wall ansatz which gains additional rotation due to the magnetic field of the vortex, i.e., $\theta(r) \approx \theta_{R,\delta}(r) + \delta\theta(r)$. To determine the rotation angle $\delta\theta(r)$, we consider the magnetization of the ferromagnet in three different regions: Near the center of the skyrmion, at $r \sim |R|$, and far from the origin. Far from or near the center of the skyrmion, the magnetization is nearly homogeneous $m_z \approx \pm 1$, and its variation is determined mostly by the magnetic field of the vortex, hence $\delta\theta(r) \approx \pm\theta_\gamma(r)$. In the intermediate region, $m_z \approx \cos\theta_{R,\delta}(r)$, such that the rotation angle $\delta\theta(r)$ can be smoothed out to give $\delta\theta(r) \approx \theta_\gamma(r)m_z = \theta_\gamma(r)\cos\theta_{R,\delta}(r)$, and we arrive at the ansatz in Eq. (5).

D. Micromagnetic modeling

In addition to the exact solution of Eq. (3) and the minimization of $\mathcal{F}[\mathbf{m}]$ with the ansatz in Eq. (5), we have run a series of micromagnetic simulations using OOMMF software [38]. We simulated the system as a set of classical magnetic vectors placed at the centers of the grid cells in the xy plane. We impose periodic boundary conditions, meaning that the

total energy on such a lattice can be taken in its continuous limit and is thus given by Eq. (1). The Pearl vortex is located at the origin $x = y = 0$. We initiate the system with the magnetization determined by the ansatz in Eq. (5).

III. RESULTS

The magnetic field of the vortex makes the free energy landscape more complicated than at $\gamma = 0$. There are regions of γ and ϵ in which several minima of $\mathcal{F}[\mathbf{m}]$ exist. To illustrate this behavior, in Fig. 1(a), we plot the shifted free energy $\Delta\mathcal{F}[R] = \mathcal{F}[R] - \mathcal{F}[R \to 0]$ normalized by the energy scale Ad_F as a function of the skyrmion radius $|R|$ for $\epsilon = 0.3$ and $\gamma = 0.522$ [39]. Here, $\mathcal{F}[R]$ is the free energy $\mathcal{F}[\mathbf{m}]$ computed with the help of the ansatz $\theta(r) = \theta_{R,\delta,\gamma}(r)$ and minimized with respect to the skyrmion wall width δ only. As can be seen in Fig. 1(a), $\Delta\mathcal{F}[R]$ has three minima: Two minima corresponding to the positive chirality $\chi = +1$ (green square and red diamond) and one minimum for negative chirality $\chi = -1$ (blue disk). These minima may potentially correspond to the skyrmion stable states (see below). We emphasize that the radius of the stable skyrmion configuration (red diamond in Fig. 1) is $R \approx 8.6\ell_w$, which is $\sim$25 times larger than the skyrmion radius $R_0 \approx 0.33\ell_w$ at $\gamma = 0$. Additionally, $\Delta\mathcal{F}[R]$ has two maxima (brown and magenta circles) which correspond to the saddlelike solutions [40] of Eq. (3).

In Fig. 1(b), we show the exact solutions of Eq. (3) (solid curves) in comparison with the instances of the ansatz (dashed curves) for the five extrema of $\Delta\mathcal{F}[R]$ in Fig. 1(a). To plot $\theta_{R,\delta,\gamma}(r)$, we use R and δ found by minimizing the free energy. There is very good agreement between the exact solution and the ansatz. We have checked that such an agreement is a general situation provided that $\gamma \lesssim 1$.

The solutions with positive chirality shown in Fig. 1 have an interesting feature. The magnetization is parallel to the z axis not only at the origin and at infinity but also at two intermediate distances [see Fig. 1(b)]. This is related to the fact that, at small distances from the origin, the magnitude of the skyrmion angle is larger than π, whereas at large distances, the angle becomes negative. Both features arise because the spatial dependence of the skyrmion angle at small and large distances is controlled by the vortex solution in Eq. (4), see dotted curves in Fig. 1(b).

By exploring different initial magnetizations in the micromagnetic modeling, we have managed to observe all three stable skyrmion profiles for $\epsilon = 0.3$ and $\gamma = 0.522$. They are shown as color-plot insets in Fig. 1. For three stable skyrmions, we have also extracted a dependence of the skyrmion angle on distance r; these are represented by symbols in Fig. 1(b). We emphasize that the exact solution of Eq. (3), the ansatz in Eq. (5), and the result of the micromagnetic simulations agree remarkably well.

As the choice of parameters ϵ and γ corresponds to a particular heterostructure, varying these parameters may cause the number of extrema in $\Delta\mathcal{F}[R]$ to change. To investigate this relationship, we show in Fig. 2 semilog dependencies of R on γ for several values of ϵ. The solid and dashed curves on the plane (γ, R) correspond to the minima and maxima of

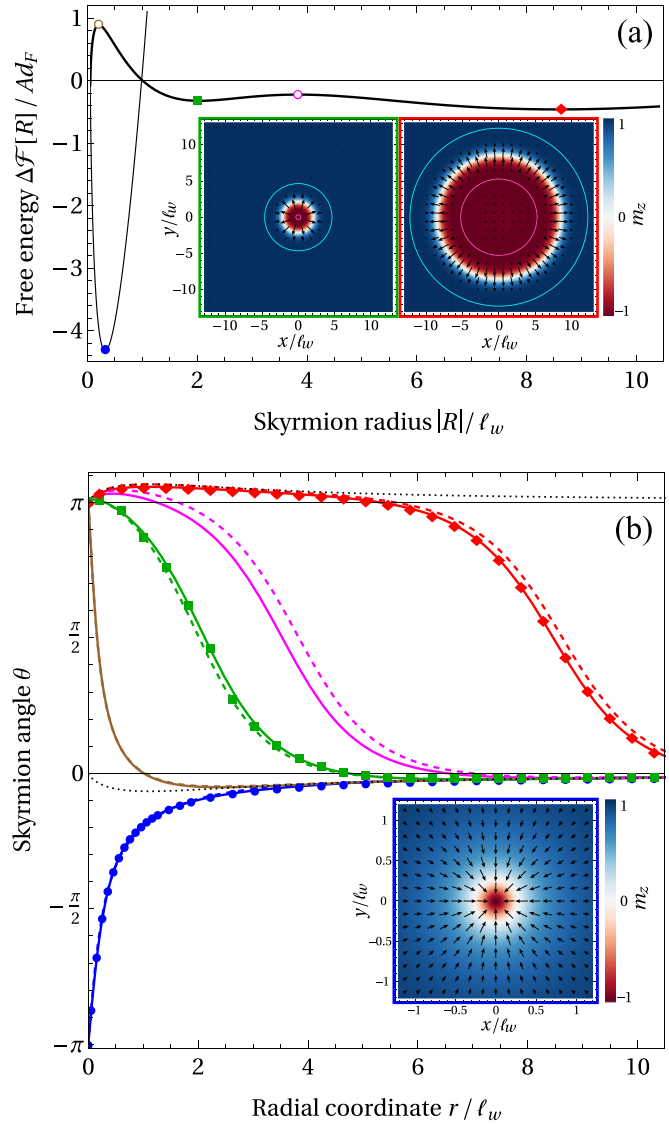

FIG. 1. (a) Dependence of shifted dimensionless free energy $\Delta\mathcal{F}[R]/(Ad_F)$ on skyrmion radius $|R|$ for $\epsilon = 0.3$ and $\gamma = 0.522$. The thicker (thinner) curve describes it for the positive (negative) chirality $\chi = +1(-1)$. The blue disk, green square, and red diamond indicate the minima of $\Delta\mathcal{F}[R]$, while the brown and magenta circles indicate the maxima. (b) The skyrmion angles $\theta(r)$ corresponding to the minima and maxima of $\Delta\mathcal{F}[R]$ from (a). The solid and dashed curves show the exact solution of Eq. (3) and the approximations given by the ansatz in Eq. (5) with $\{R, \delta\}/\ell_w \approx \{-0.28, 0.78\}$, $\{0.16, 0.62\}$, $\{2.0, 0.91\}$, $\{3.8, 0.96\}$, and $\{8.6, 0.99\}$, respectively. The functions $\theta_\gamma(r)$ and $\pi - \theta_\gamma(r)$ are plotted as the black dotted curves. The points marked by blue disks, green squares, and red diamonds are extracted from the micromagnetic modeling. Insets: The spatial distribution of magnetization for stable skyrmion states is obtained by micromagnetic simulations. The colors of the inset frames correspond to the color of the curves $\theta(r)$ of (b). The color gradient indicates the magnitude of the z component of magnetization (see color bar). The black arrows guide the magnitude and direction of the in-plane magnetization. The pink and cyan curves shown in the insets in (a) (green and red frames) correspond to the distances from the center at which $m_r = 0$.

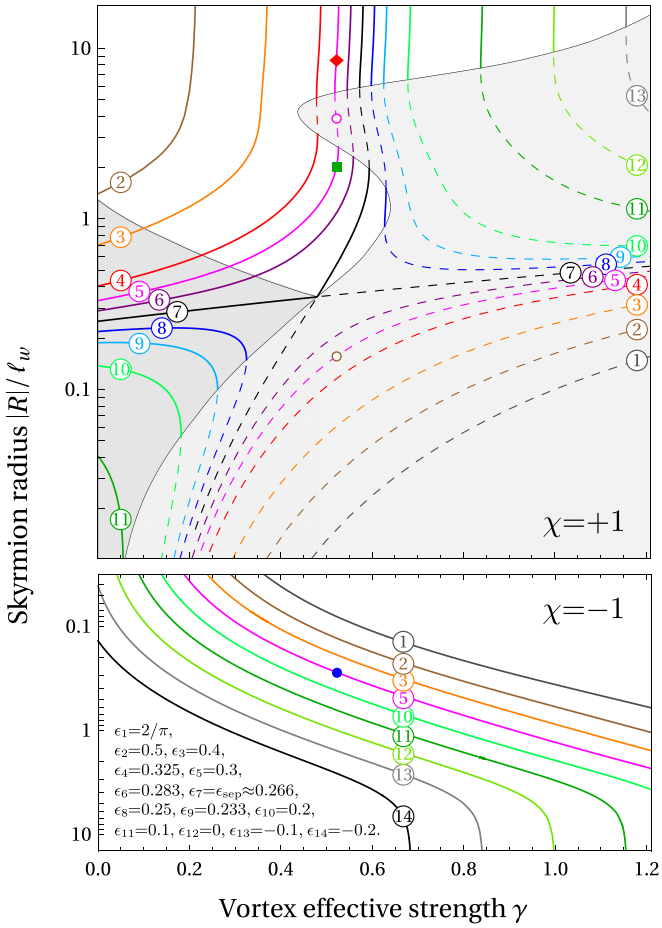

FIG. 2. Dependence of skyrmion radius $|R|/\ell_w$ on the effective vortex strength γ for several values of DMI parameter ϵ in semilog scale for chiralities $\chi = \pm 1$. The solid and dashed curves correspond to the minima and maxima of $\Delta\mathcal{F}[R]$, respectively. The area of unstable coaxial states and the area of metastable states are marked by the darker and lighter gray fillings, respectively. The values of ϵ used for the curves with the corresponding numbers from 1 to 14 are provided in the lower panel. The blue disk, green square, and red diamond correspond to the stable skyrmions in Fig. 1, while the brown and magenta circles show the solutions corresponding to maxima of $\Delta\mathcal{F}[R]$ there.

$\Delta\mathcal{F}[R]$, respectively. The extent of the saddlelike metastable states is marked by the lighter gray filling in Fig. 2.

Both the exact solution of Eq. (3) and the relevant instances of the ansatz in Eq. (5) give stable skyrmions, provided that the skyrmion center coincides with the center of the Pearl vortex. However, these states can be unstable due to the fact that, for particular ϵ and γ, the skyrmion center can shift from the center of the vortex. As is shown in Ref. [29], a skyrmion-vortex pair can remain stable when the skyrmion is located at some finite distance a from the Pearl vortex. To determine the stability of the coaxial configuration, we shift the skyrmion from the center to the infinitesimally small distance $a \to 0$ and compare the free energy of the shifted and coaxial configurations. The corresponding analysis [41] shows that coaxial skyrmion-vortex states with chirality $\chi = +1$ for $\epsilon < \epsilon_{cr} \approx 0.49$ and $\gamma < \gamma_{cr}(\epsilon)$ are unstable, in which case the skyrmion is repulsed from the vortex. If any of the above conditions are not satisfied, the coaxial configuration appears to be stable with respect to the shifting. In Fig. 2, we mark the area of the unstable configurations by the darker gray filling, while the white background indicates the stable coaxial configurations.

The diagram in Fig. 2 has several interesting features. Firstly, all curves for skyrmions of chirality $\chi = +1$ (the upper panel) are located in quadrants which are produced on the plane (γ, R) by the curve at $\epsilon = \epsilon_{sep} \approx 0.266$ (black line #7). For $\epsilon < \epsilon_{sep}$, curves $R(\gamma)$ are located in the left-bottom and right-top quadrants, while the curves for $\epsilon > \epsilon_{sep}$ are situated in the right-bottom and left-top quadrants. We emphasize that, even for $\epsilon \leqslant 0$, there are skyrmions with $\chi = +1$ in the right-top quadrant (see curves #12 and #13).

Secondly, for $0.25 \lesssim \epsilon \lesssim 0.35$, there are values of γ where two skyrmions of chirality $\chi = +1$ may exist. An example of this situation can be seen in Fig. 1(a), in which the solid curve displays two minima of $\Delta\mathcal{F}[R]$ which correspond to positive chirality.

Thirdly, for each pair of ϵ and γ, there is a skyrmion of chirality $\chi = -1$ with a certain radius $|R|$, see the lower panel of Fig. 2. However, it should be emphasized that, for small γ and $\epsilon > 0$, the skyrmion radius appears to be extremely small ($R \lll \ell_w$). In this case, Eq. (1) is no longer valid, and thus, solutions with such small radii are not included in Fig. 2. As can be clearly seen in Fig. 2, the radius $|R|$ for the skyrmions with $\chi = -1$ increases monotonically with the growth of γ.

Finally, for each ϵ and for both chiralities $\chi = \pm 1$, there exists a critical value $\gamma_\pm(\epsilon)$. When an increasing γ approaches $\gamma_\pm$, the skyrmion radius grows significantly. For $|R| \gg \ell_w$, the free energy can be calculated in the leading approximation:

$$\frac{\Delta\mathcal{F}[R]}{8\pi A d_f} \approx \frac{(1 \mp \epsilon\pi/2)|R|}{\ell_w} - \gamma \ell_w^{-2} \int_0^{|R|} dr\, r b_z(r). \qquad (7)$$

The first term involves the energy of the domain wall separating the interior and exterior skyrmion regions, while the second term comes from the energy of the inner skyrmion region in which magnetization $m_z \approx -1$ is directed opposite to the magnetization in the ferromagnetic state $m_z \approx +1$. For $\ell_w \ll |R| \ll \lambda$, we can approximate $b_z(r) \approx \ell_w/r$ and estimate the second term in Eq. (7) as $\gamma|R|/\ell_w$. Therefore, the critical value of γ can be estimated as $\gamma_\pm(\epsilon) \approx 1 \mp \epsilon\pi/2 > 0$. If $\gamma \gtrsim \gamma_\pm$, the skyrmion radius becomes comparable or larger than the Pearl length $|R| \gtrsim \lambda \gg \ell_w$, and the minimum of $\Delta\mathcal{F}[R]$ is determined by the relation $|R| b_z(|R|) \approx \ell_w \gamma_\pm/\gamma$. For $\gamma \gg \gamma_\pm$, we can approximate the magnetic field of the vortex as $b_z(|R|) \approx 4\ell_w\lambda^2/|R|^3$ at $|R| \gg \lambda$. Therefore, the minimum of $\Delta\mathcal{F}[R]$ occurs at $|R| \approx 2\lambda\sqrt{\gamma/\gamma_\pm}$.

IV. DISCUSSION

As shown in Fig. 2, the most interesting effects are predicted to occur in the range $\epsilon = 0.25 \div 0.45$ and $\gamma = 0.3 \div 0.7$. However, in the SF heterostructures which have been studied experimentally thus far [23,42–47], ϵ varies from 0.25 to 0.45, whereas $\gamma \lesssim 0.1$ due to the large magnitude of the Pearl penetration length. Therefore, to observe the effects predicted here, γ should be enlarged by increasing d_S, and cleaner superconductors should be used to reduce λ_L.

Our results imply that a superconducting vortex stabilizes a Néel-type skyrmion in the absence of DMI, as shown by the curve #12 in Fig. 2 (for a similar effect in the absence of a vortex, see Ref. [48]).

We note that experiments are usually performed under an external out-of-plane magnetic field. Such a field can be readily incorporated into our approach [49]. In addition, the case of an antivortex ($\gamma < 0$) cannot be easily related to the case $\gamma > 0$ via a simple symmetry transformation and, therefore, requires separate investigation [49]. Finally, our theory can be extended to skyrmions and vortices in confined geometries [50–52], skyrmion-vortex lattices [53], and more exotic topological spin textures [7], such as bimerons [54] and antiferromagnetic skyrmions [55].

V. SUMMARY

Using three complementary approaches, namely, the exact numerical solution of the Euler-Lagrange equation in Eq. (3), the free energy minimization with two-parameter ansatz in Eq. (5), and micromagnetic simulations, we have developed a theory of the magnetization profile for the coaxial configuration of the Néel-type skyrmion and the Pearl vortex in thin superconductor-chiral ferromagnetic heterostructures. We have found that the inhomogeneous magnetic field of the Pearl vortex significantly influences the skyrmion profile, leading to drastic enhancement of the radius of the skyrmion (experimental indication of which has been recently reported in a weak parameter range [56]) and inversion of the chirality of the skyrmion. Both effects are controlled by the dimensionless magnetic field strength γ, which is proportional to the thickness of the superconductor d_S. Such a significant modification of the skyrmion magnetization profile in the presence of a vortex can affect Majorana modes localized at skyrmion-vortex pairs [14–21].

ACKNOWLEDGMENTS

We thank C. Panagopoulos, A. Fraerman, M. Kuznetsov, and M. Shustin for useful discussions. We are grateful to L. Cobus for the careful reading of the manuscript. The work of S.S.A., E.S.A., and I.S.B. was funded by the Russian Science Foundation under Grant No. 21-42-04410. O.A.T. acknowledges the support by the Australian Research Council (Grant No. DP200101027); the Cooperative Research Project Program at the Research Institute of Electrical Communication, Tohoku University (Japan); and an NCMAS grant.

[1] V. V. Ryazanov, V. A. Oboznov, A. S. Prokofiev, V. V. Bolginov, and A. K. Feofanov, Superconductor-ferromagnet-superconductor π-junctions, J. Low Temp. Phys. **136**, 385 (2004).

[2] I. F. Lyuksyutov and V. L. Pokrovsky, Ferromagnet-superconductor hybrids, Adv. Phys. **54**, 67 (2005).

[3] A. I. Buzdin, Proximity effects in superconductor-ferromagnet heterostructures, Rev. Mod. Phys. **77**, 935 (2005).

[4] F. S. Bergeret, A. F. Volkov, and K. B. Efetov, Odd triplet superconductivity and related phenomena in superconductor-ferromagnet structures, Rev. Mod. Phys. **77**, 1321 (2005).

[5] M. Eschrig, Spin-polarized supercurrents for spintronics: A review of current progress, Rep. Prog. Phys. **78**, 104501 (2015).

[6] C. Back, V. Cros, H. Ebert, K. Everschor-Sitte, A. Fert, M. Garst, T. Ma, S. Mankovsky, T. L. Monchesky, M. Mostovoy *et al.*, The 2020 skyrmionics roadmap, J. Phys. D: Appl. Phys. **53**, 363001 (2020).

[7] B. Göbel, I. Mertig, and O. A. Tretiakov, Beyond skyrmions: Review and perspectives of alternative magnetic quasiparticles, Phys. Rep. **895**, 1 (2021).

[8] A. O. Zlotnikov, M. S. Shustin, and A. D. Fedoseev, Aspects of topological superconductivity in 2D systems: Non-collinear magnetism, skyrmions, and higher-order topology, J. Supercond. Nov. Magn. **34**, 3053 (2021).

[9] A. N. Bogdanov and D. Yablonskii, Thermodynamically stable "vortices" in magnetically ordered crystals. the mixed state of magnets, Zh. Eksp. Teor. Fiz. **95**, 178 (1989) [Sov. Phys. JETP **68**, 101 (1989)].

[10] S. S. Pershoguba, S. Nakosai, and A. V. Balatsky, Skyrmion-induced bound states in a superconductor, Phys. Rev. B **94**, 064513 (2016).

[11] K. Pöyhönen, A. Weststrom, S. S. Pershoguba, T. Ojanen and A. V. Balatsky, Skyrmion-induced bound states in a p-wave superconductor, Phys. Rev. B **94**, 214509 (2016).

[12] T. Yokoyama and J. Linder, Josephson effect through magnetic skyrmions, Phys. Rev. B **92**, 060503(R) (2015).

[13] V. A. Tumanov, V. E. Zaitseva, and Yu. N. Proshin, Critical temperature of a superconductor/ferromagnet nanostructure near a magnetic skyrmion, JETP Lett. **116**, 449 (2022).

[14] W. Chen and A. P. Schnyder, Majorana edge states in superconductor-noncollinear magnet interfaces, Phys. Rev. B **92**, 214502 (2015).

[15] G. Yang, P. Stano, J. Klinovaja, and D. Loss, Majorana bound states in magnetic skyrmions, Phys. Rev. B **93**, 224505 (2016).

[16] U. Güngördü, S. Sandhoefner, and A. A. Kovalev, Stabilization and control of Majorana bound states with elongated skyrmions, Phys. Rev. B **97**, 115136 (2018).

[17] E. Mascot, S. Cocklin, S. Rachel, and D. K. Morr, Dimensional tuning of Majorana fermions and real space counting of the Chern number, Phys. Rev. B **100**, 184510 (2019).

[18] S. Rex, I. V. Gornyi, and A. D. Mirlin, Majorana bound states in magnetic skyrmions imposed onto a superconductor, Phys. Rev. B **100**, 064504 (2019).

[19] M. Garnier, A. Mesaros, and P. Simon, Topological superconductivity with deformable magnetic skyrmions, Commun. Phys. **2**, 126 (2019).

[20] S. Rex, I. V. Gornyi, and A. D. Mirlin, Majorana modes in emergent-wire phases of helical and cycloidal magnet-superconductor hybrids, Phys. Rev. B **102**, 224501 (2020).

[21] U. Güngördü and A. A. Kovalev, Majorana bound states with chiral magnetic textures, J. Appl. Phys. **132**, 041101 (2022).

[22] J. Nothhelfer, S. A. Díaz, S. Kessler, T. Meng, M. Rizzi, K. M. D. Hals, and K. Everschor-Sitte, Steering Majorana braiding via skyrmion-vortex pairs: A scalable platform, Phys. Rev. B **105**, 224509 (2022).

[23] A. P. Petrović, M. Raju, X. Y. Tee, A. Louat, I. Maggio-Aprile, R. M. Menezes, M. J. Wyszyński, N. K. Duong, M. Reznikov, Ch. Renner *et al.*, Skyrmion-(Anti)Vortex Coupling in a Chiral

Magnet-Superconductor Heterostructure, Phys. Rev. Lett. **126**, 117205 (2021).
[24] K. M. D. Hals, M. Schecter, and M. S. Rudner, Composite Topological Excitations in Ferromagnet-Superconductor Heterostructures, Phys. Rev. Lett. **117**, 017001 (2016).
[25] J. Baumard, J. Cayssol, F. S. Bergeret, and A. Buzdin, Generation of a superconducting vortex via Néel skyrmions, Phys. Rev. B **99**, 014511 (2019).
[26] S. M. Dahir, A. F. Volkov, and I. M. Eremin, Interaction of Skyrmions and Pearl Vortices in Superconductor-Chiral Ferromagnet Heterostructures, Phys. Rev. Lett. **122**, 097001 (2019).
[27] R. M. Menezes, J. F. S. Neto, C. C. de Souza Silva, and M. V. Milošević, Manipulation of magnetic skyrmions by superconducting vortices in ferromagnet-superconductor heterostructures, Phys. Rev. B **100**, 014431 (2019).
[28] S. M. Dahir, A. F. Volkov, and I. M. Eremin, Meissner currents induced by topological magnetic textures in hybrid superconductor/ferromagnet structures, Phys. Rev. B **102**, 014503 (2020).
[29] E. S. Andriyakhina and I. S. Burmistrov, Interaction of a Néel-type skyrmion with a superconducting vortex, Phys. Rev. B **103**, 174519 (2021).
[30] The demagnetizing field contribution is included in the effective perpendicular anisotropy constant $K = K_0 - 2\pi M_s^2$ [27,29,48].
[31] J. Pearl, Current distribution in superconducting films carrying quantized fluxoids, Appl. Phys. Lett. **5**, 65 (1964).
[32] G. Carneiro and E. H. Brandt, Vortex lines in films: Fields and interactions, Phys. Rev. B **61**, 6370 (2000).
[33] See Supplemental Material at http://link.aps.org/supplemental/10.1103/PhysRevB.107.L220409 for the details of the magnetic field of the Pearl vortex and micromagnetic framework.
[34] In fact, this behavior holds for $\lambda_L \ll r \ll \lambda$. At smaller distances $r \ll \lambda_L$, one finds $b_r(r) \propto \ell_w r/\lambda_L^2$ and $b_z(r) \propto \ell_w/\lambda_L$, but region $r \ll \lambda_L$ is not important for our solution for θ_γ [33].
[35] To derive the analytical result of Eq. (4), we assume $\theta_\gamma(r)$ to be small and linearize Eq. (3). The maximal absolute value of $\theta_\gamma(r)$ equals $\sim 0.4\gamma$. Therefore, Eq. (4) is correct provided $\gamma \lesssim 1$.
[36] A. Bogdanov and A. Hubert, Thermodynamically stable magnetic vortex states in magnetic crystals, J. Magn. Magn. Mater. **138**, 255 (1994).
[37] However, as the ferromagnet with $|\epsilon| > 2/\pi$ is in a spiral rather than homogeneous state, the case of such a strong DMI is thus not of interest for this letter.
[38] M. J. Donahue and D. G. Porter, OOMMF User's Guide, Version 1.0, Tech. Rep. (Interagency Report NISTIR, 1999).
[39] Value $\gamma = 0.522$ is taken with such high precision because the skyrmion radius is sensitive to the vortex strength in this range of parameters. Indeed, changing γ by 1% may vary radius R by up to 10%.
[40] We term some solutions of the Euler-Lagrange Eq. (3) as saddlelike solutions because they correspond to the saddle points of free energy $\mathcal{F}$ as functions of two skyrmion parameters R and δ. Namely, at these points, $\mathcal{F}[R, \delta]$ have a minimum as a function of δ and a maximum as a function of R.
[41] E. S. Andriyakhina, S. S. Apostoloff, and I. S. Burmistrov, Repulsion of a Néel-type skyrmion from a Pearl vortex in thin ferromagnet-superconductor heterostructures, JETP Lett. **116**, 825 (2022).
[42] P. J. Metaxas, J. P. Jamet, A. Mougin, M. Cormier, J. Ferré, V. Baltz, B. Rodmacq, B. Dieny, and R. L. Stamps, Creep and Flow Regimes of Magnetic Domain-Wall Motion in Ultrathin Pt/Co/Pt Films with Perpendicular Anisotropy, Phys. Rev. Lett. **99**, 217208 (2007).
[43] J. Sampaio, V. Cros, S. Rohart, A. Thiaville, and A. Fert, Nucleation, stability and current-induced motion of isolated magnetic skyrmions in nanostructures, Nat. Nanotechnol. **8**, 839 (2013).
[44] N. Romming, C. Hanneken, M. Menzel, J. E. Bickel, B. Wolter, K. von Bergmann, A. Kubetzka, and R. Wiesendanger, Writing and deleting single magnetic skyrmions, Science **341**, 636 (2013).
[45] K.-S. Ryu, S.-H. Yang, L. Tomas, and S. S. P. Parkin, Chiral spin torque arising from proximity-induced magnetization, Nat. Commun. **5**, 3910 (2014).
[46] N. Romming, A. Kubetzka, C. Hanneken, K. von Bergmann, and R. Wiesendanger, Field-Dependent Size and Shape of Single Magnetic Skyrmions, Phys. Rev. Lett. **114**, 177203 (2015).
[47] C. Moreau-Luchaire, C. Moutafis, N. Reyren, J. Sampaio, C. A. F. Vaz, N. Van Horne, K. Bouzehouane, K. Garcia, C. Deranlot, P. Warnicke *et al.*, Additive interfacial chiral interaction in multilayers for stabilization of small individual skyrmions at room temperature, Nat. Nanotechnol. **11**, 444 (2016).
[48] M. A. Kuznetsov, K. R. Mukhamatchin, and A. A. Fraerman, Effective interfacial Dzyaloshinskii-Moriya interaction and skyrmion stabilization in ferromagnet/paramagnet and ferromagnet/superconductor hybrid systems, Phys. Rev. B **107**, 184428 (2023).
[49] The correspondent studies will be published elsewhere.
[50] S. Rohart and A. Thiaville, Skyrmion confinement in ultrathin film nanostructures in the presence of Dzyaloshinskii-Moriya interaction, Phys. Rev. B **88**, 184422 (2013).
[51] V. L. Vadimov, M. V. Sapozhnikov, and A. S. Mel'nikov, Magnetic skyrmions in ferromagnet-superconductor (F/S) heterostructures, Appl. Phys. Lett. **113**, 032402 (2018).
[52] L. González-Gómez, J. Castell-Queralt, N. Del-Valle, and C. Navau, Mutual Interaction between Superconductors and Ferromagnetic Skyrmionic Structures in Confined Geometries, Phys. Rev. Appl. **17**, 034069 (2022).
[53] J. F. Neto and C. C. de Souza Silva, Mesoscale Phase Separation of Skyrmion-Vortex Matter in Chiral-Magnet–Superconductor Heterostructures, Phys. Rev. Lett. **128**, 057001 (2022).
[54] B. Göbel, A. Mook, J. Henk, I. Mertig, and O. A. Tretiakov, Magnetic bimerons as skyrmion analogues in in-plane magnets, Phys. Rev. B **99**, 060407(R) (2019).
[55] J. Barker and O. A. Tretiakov, Static and Dynamical Properties of Antiferromagnetic Skyrmions in the Presence of Applied Current and Temperature, Phys. Rev. Lett. **116**, 147203 (2016).
[56] P. Machain, Skyrmion-Vortex Interactions in Chiral-Magnet/Superconducting Hybrid Systems, Ph.D. thesis, Nanyang Technological University, Singapore, 2021.